

# Testing the Role of Radiation in Determining Tropical Cloud-Top Temperature

BRYCE E. HARROP AND DENNIS L. HARTMANN

*Department of Atmospheric Sciences, University of Washington, Seattle, Washington*

(Manuscript received 10 August 2011, in final form 14 February 2012)

## ABSTRACT

A cloud-resolving model is used to test the hypothesis that radiative cooling by water vapor emission is the primary control on the temperature of tropical anvil clouds. The temperature of ice clouds in the simulation can be increased or decreased by changing only the emissivity of water vapor in the upper troposphere. The effect of the model's fixed ozone profile on stability creates a pressure-dependent inhibition of convection, leading to a small warming in cloud-top temperature as SST is increased. Increasing stratospheric water vapor also warms the cloud-top temperature slightly. Changing the latent heat of fusion reduces the cloud fraction at high altitudes, but does not significantly change temperature at which cloud fraction peaks in the upper troposphere. The relationship between radiatively driven horizontal mass convergence and cloud fraction that causes cloud temperature to be insensitive to surface temperature is preserved when a large model domain is used so that convection aggregates in a small part of the model domain.

## 1. Introduction

Climate feedbacks involving water vapor and clouds are very important for the magnitude and structure of climate change, and the strongest energy exchanges are in the tropics. Hartmann and Larson (2002) proposed a constraint on the temperature of tropical anvil clouds derived from the Clausius–Clapeyron relation and the emission lines of water vapor. This so called “fixed anvil temperature” (FAT) hypothesis suggests that the temperature where anvil clouds detrain is tied to the same temperature where the relaxation time scale of clear-sky radiative cooling diminishes. The temperature at which saturation vapor pressure becomes small enough that water vapor is an ineffective radiator is narrowly constrained by the Clausius–Clapeyron relation and is very insensitive to surface temperature. Because water vapor is the principal contributor to the cooling of the atmosphere, as water vapor concentrations decline with temperature in the upper troposphere, so must the efficiency of atmospheric cooling by radiative emission. Hartmann et al. (2001) demonstrated that the transition to low vapor emissions currently occurs near 200 mb, well below the tropical cold point tropopause. Observations

also show that anvil clouds detrain at around 200 mb or about 218 K (Houze and Betts 1981). Saturation water vapor concentration is purely a function of temperature by the Clausius–Clapeyron relationship. Thus, the atmosphere's ability to cool itself declines as a function of temperature (if relative humidity remains constant), and the FAT hypothesis predicts that anvil cloud emission temperatures will be very insensitive to surface temperature, giving a strong longwave cloud feedback.

The FAT hypothesis has been examined in both modeling and observational studies. Model studies seeking to test the FAT hypothesis have shown cloud-top temperatures to be invariant to changes in sea surface temperature (Hartmann and Larson 2002; Kuang and Hartmann 2007). An earlier study testing tropical convection sensitivity to sea surface temperature in a cloud-resolving model had shown cloud-top temperatures warm with increasing SSTs (Tompkins and Craig 1999). However, Kuang and Hartmann (2007) argued that the 1-km vertical resolution of the model used by Tompkins and Craig (1999) was insufficient for testing the FAT hypothesis.

Observational studies have attempted to measure the cloud-top temperature response to SST. Sea surface temperature changes due to El Niño are a natural test for model predictions. Xu et al. (2007) and Eitzen et al. (2009) used Clouds and the Earth's Radiant Energy System (CERES) data from the 1998 El Niño to observe

---

*Corresponding author address:* Bryce E. Harrop, Dept. of Atmospheric Sciences, University of Washington, Box 351640, Seattle, WA 98195-1640.  
E-mail: bryce@atmos.washington.edu

how cloud-top temperature changes with sea surface temperature. Sorting by sea surface temperature yielded significantly different cloud-top temperatures—which the authors suggested were due, in part, to differing large-scale dynamical patterns. If, however, the data were sorted by the precession cycle of the CERES satellite, the cloud-top temperature did not depend on sea surface temperature—even though the sea surface temperatures between precession cycles were found to be significantly different (Xu et al. 2007; Eitzen et al. 2009). “Precession cycle” refers to the 46-day period over which the Tropical Rainfall Measuring Mission (TRMM) satellite completes its sampling of the diurnal cycle at a given location.

The radiatively driven horizontal mass convergence can be calculated following Kuang and Hartmann (2007):

$$-\nabla_H \cdot \mathbf{v} = \frac{\partial \omega}{\partial p} = \frac{\partial}{\partial p} \left( \frac{Q_{\text{clr}}}{\sigma} \right), \quad (1)$$

where  $-\nabla_H \cdot \mathbf{v}$  is the horizontal convergence of velocity,  $\omega$  is the pressure velocity,  $p$  is the pressure,  $Q_{\text{clr}}$  is the clear-sky heating rate (negative for cooling; averaged over clear-sky columns only), and  $\sigma = -(T/\theta)(\partial\theta/\partial p)$  is the static stability. The decline in water vapor cooling in the clear-sky results in the above radiatively driven mass convergence in the clear sky. The FAT hypothesis suggests that divergence in the convectively active regions—needed to preserve mass continuity—is what determines the detrainment level of the anvil clouds. In short, the FAT hypothesis suggests that the anvil cloud detrainment temperature is determined by the radiative cooling due to water vapor and must, therefore, be very nearly fixed.

Kubar et al. (2007) showed a strong correspondence between radiatively driven mass convergence and anvil cloud temperatures measured by the Moderate Resolution Imaging Spectroradiometer (MODIS). Colder anvil cloud temperatures were found in the western tropical Pacific, as compared to the eastern tropical Pacific (Kubar et al. 2007). The anvil temperature differences were attributed to differences in upper-tropospheric ( $\sim 200$  mb) humidity between the two regions. Radiatively driven mass convergence also peaked at a warmer temperature in the eastern Pacific because of both reduced humidity and enhanced stability. An analysis of data from the Multi-angle Imaging SpectroRadiometer (MISR) revealed differences in anvil cloud-top temperature linked to changes in stability near and above the outflow height (Chae and Sherwood 2010). Chae and Sherwood (2010) also demonstrated, using a simple statistical model, that the change in cloud-top temperature

is independent of any differences in lapse rate in layers below 10.5 km or 200 mb. Zelinka and Hartmann (2010) showed that the tropical clouds in Intergovernmental Panel on Climate Change Fourth Assessment Report (AR4) models rise with a warming climate following the radiatively driven clear-sky mass convergence, and that this explains the consistently positive longwave cloud feedback in the AR4 models. They proposed a refinement of the FAT hypothesis: the Proportionately Higher Anvil Temperature (PHAT) hypothesis. Like the FAT hypothesis, the PHAT hypothesis predicts anvil cloud detrainment to occur at the same level as the clear-sky mass convergence. This clear-sky convergence level, however, is not necessarily at a fixed temperature. Zelinka and Hartmann (2011) used a suite of satellites to compare clear-sky radiatively driven mass convergence and observed anvil clouds in the tropics. They found agreement between the retrieved cloud fraction and the calculated clear-sky radiative convergence (using cooling profiles calculated with the Fu–Liou radiative transfer code (Fu and Liou 1992) with retrieved temperature and humidity profiles as inputs). Zelinka and Hartmann (2011) found that the data were consistent with clouds rising to lower pressures while remaining essentially the same temperature as SST increased during El Niño.

Models and data suggest a strong link between radiatively driven mass convergence and cloud fraction. There remains some question whether water vapor cooling determines the temperature where the radiatively driven mass convergence and cloud fraction peak. We address that question here by changing only the radiative cooling of water vapor in a cloud-resolving model. We modify the emissivity of water vapor in the upper troposphere and look for changes in the cloud-top temperature. The FAT hypothesis predicts cloud-top temperatures will increase when we decrease water vapor emissivity in the upper troposphere, and vice versa. Also, the change in cloud-top temperature should follow a similar change in the radiatively driven clear-sky mass convergence. We show the anvil clouds detrain where the radiative cooling of water vapor weakens. This link supports the FAT hypothesis: the clouds, and consequently the cloud tops, rise in altitude to remain at nearly constant temperature even as the surface temperature rises.

We also address the evidence suggesting vertical static stability in the upper troposphere as a factor in determining cloud-top temperature (Chae and Sherwood 2010; Zelinka and Hartmann 2010). While we show that the cloud-top temperatures are quite similar under changing sea surface temperature, slight variations exist and are consistent with the idea that stronger stability

suppresses the rise of cloud tops, resulting in small increases in the cloud-top temperature as the surface warms. Of course stability is determined by a combination of radiative heating and convection. We show that in our model the warmer cloud tops are due to the radiative heating of ozone, whose concentration is a function only of pressure.

We also examine the sensitivity of cloud temperature to factors other than water vapor. Additional simulations involve modifying other radiatively active gases. We make modifications aimed at testing the relative contributions of ozone and carbon dioxide to the radiatively driven mass convergence and cloud detrainment levels. We find that removal of non-water-vapor trace gases, especially ozone, cools the clouds through changes in radiative cooling profiles and their effect on stability. We also remove the clouds from the radiative transfer calculation to see what impact the radiative effects of clouds have for their own development. We show that radiative interactions with clouds serve to alter the clouds' areal extent, but not the temperature level at which they detrain.

Stratospheric water vapor may also play a non-negligible role in determining the emissive temperature of clouds in the upper tropical troposphere. Oman et al. (2008) showed that sea surface temperature, ozone, and large-scale ascent are all important in determining the cold point tropopause temperature and hence the entry value for stratospheric water vapor. They further suggest that models with fixed ozone profiles may be biased toward warmer cold point temperatures for increasing sea surface temperatures. Chemistry–climate models tend to have difficulty predicting the cold point temperature (Pawson et al. 2000; Eyring et al. 2006), suggesting that model-predicted stratospheric water vapor has similar uncertainty. To determine the role of stratospheric water vapor in our model, we fix its value during the simulations. We investigate the constraint of fixing the stratospheric water vapor by comparing the base concentration (3.5 ppmv) to the doubled concentration (7 ppmv). We show that the higher concentration of water vapor in the stratosphere warms the clouds because of increased downwelling longwave radiation. This warming is consistent with a warming upper troposphere shown in a GCM study investigating increases in stratospheric water vapor (Rind and Lonergan 1995).

Another alternative explanation for the insensitivity of cloud temperature to sea surface temperature is that the latent heating from condensation and fusion declines with temperature, thus reducing the lifting capacity of saturated parcels. It is plausible that an increase in the parcel latent energy could lift the clouds above the level of clear-sky cooling and force the detraining anvil

temperature to be colder than normal. To achieve greater parcel energy, we double the value of the latent heat of fusion. We demonstrate that the additional parcel energy does not go into further lifting, but instead the extra energy goes into heating the atmosphere and enhancing the stability. We show that this enhanced stability is sufficient to reduce the cloud amounts at high altitudes, but does not change the temperature at which the cloud fraction peaks.

Finally, we seek to address the mesoscale circulation between the nonconvective and convective regions and its role in determining cloud-top temperature. The FAT hypothesis asserts that the radiative cooling of water vapor in the clear-sky determines the level at which anvil clouds detrain. Following FAT, even if the convective and nonconvective regions are separated from each other by convection aggregation, the anvil detrainment should continue to follow the radiatively driven mass convergence in the clear sky. Aggregation is achieved following Bretherton et al. (2005). We run this set of experiments for the same sea surface temperatures used above, and also make the modifications to water vapor emissivity described above, to test if self-aggregated convection behaves differently. We find aggregation shows a strong coupling of the clear and convective regions, supporting the FAT hypothesis.

Because the FAT hypothesis only makes predictions for the upper-tropospheric tropical clouds, we will restrict our discussion to only this cloud type.

## 2. Model details and simulation design

The model used for this study is the System for Atmospheric Modeling (SAM) version 6.7 cloud-resolving model (Khairoutdinov and Randall 2003). The model uses the anelastic equations of motion and has a doubly periodic domain. The vertical grid is stretched with 96 levels, a rigid lid, and Newtonian damping in the upper third to suppress wave reflection. A uniform, 96 km  $\times$  96 km horizontal grid with 1-km resolution is used in the base experiments. We change the horizontal grid to 576 km  $\times$  576 km with 3-km resolution for the self-aggregation experiments. The prognostic thermodynamic variables SAM uses are liquid water/ice moist static energy, total nonprecipitating water (water vapor, cloud water, and cloud ice), and total precipitating water (rain, snow, and graupel). Monin–Obukhov similarity is used for the surface flux computations. A Rapid and Accurate Radiative Transfer Model (RRTM) is used for the radiative transfer calculation (Mlawer et al. 1997). Note this radiative transfer model is different from that used by Kuang and Hartmann (2007). All simulations are run to radiative–convective equilibrium (RCE).

We seek to change the radiative properties of water vapor without directly changing the model-predicted water vapor values. Under normal operation, the water vapor concentration passed to the radiation code is identical to the model-predicted water vapor. We change the water vapor passed to the radiation code from the model-predicted value to a value that is either reduced or increased in the upper troposphere. The increase (decrease) of water vapor has the effect of increasing (decreasing) longwave emission in the upper troposphere. Essentially, adding or removing water vapor produces the same effect as changing the absorption bands of water vapor without having to rerun the line-by-line calculations for the radiation code. Beer's law states that absorption and emission depend on the product of the absorber amount with its absorption coefficient, so either can be changed to produce the desired effect. The modifications to the radiative water vapor concentration are explained further below. Note that all microphysics calculations are done with the model-predicted water vapor.

Unless specified otherwise, the stratospheric value of water vapor is fixed at a constant 3.5 ppmv. In the model, the stratosphere is considered to be all levels above the cold point tropopause. The first simulation is designed to reduce the ability of water vapor to cool in the upper troposphere. Above a specified level, water vapor is ramped down to the stratospheric value using a half cosine function to smooth the transition as follows:

$$q_{v,RAD} = q_{v,STRAT} + H_1(T)(q_{v,MODEL} - q_{v,STRAT}), \quad (2)$$

$$H_1(T) = \frac{1}{2} \left[ 1 + \cos \left( \pi \frac{T - T_1}{T_{cp} - T_1} \right) \right], \quad (3)$$

where  $q_{v,RAD}$  is the water vapor passed to the radiation code,  $q_{v,MODEL}$  is the model-predicted water vapor,  $q_{v,STRAT}$  is the stratospheric water vapor value,  $T_{cp}$  is the temperature at the cold point tropopause, and  $T_1$  is a specified temperature to begin the transition in water vapor. Simulations where water vapor was added instead of removed were also performed. The form of the addition modification is as follows:

$$q_{v,RAD} = q_{v,STRAT} + H_2(T)(q_{v,MODEL} - q_{v,STRAT}) + K[1 - H_1(T)](q_{v,MODEL} - q_{v,STRAT}), \quad (4)$$

$$H_2(T) = \frac{1}{2} \left[ 1 + \cos \left( \pi \frac{T - T_{cp}}{T_2 - T_{cp}} \right) \right], \quad (5)$$

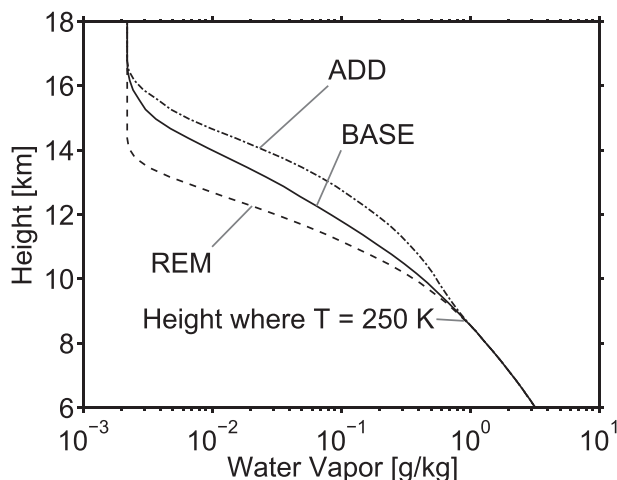


FIG. 1. Water vapor modification diagram. The different lines show the BASE (solid), REM (dashed), and ADD (dashed-dotted). For both REM and ADD,  $T_1 = 250$  K, and for ADD  $T_2 = 220$  K and  $K = 2$ .

where  $H_1(T)$  is the same as in Eq. (3),  $T_2$  is a specified temperature to end the increase in water vapor, and  $K$  is a factor by which to increase water vapor at the cold point tropopause level. Figure 1 shows the water vapor profiles resulting from the modifications described by Eqs. (2) and (4).

Table 1 provides a description of each of the runs performed for this study. For runs performed with the  $96 \text{ km} \times 96 \text{ km}$  domain, the model takes 50 days to reach RCE. Unless specifically noted otherwise, all figures will be temporally averaged spanning only the times when the model is in RCE—these times are listed in Table 1 in the “averaged days” column. Note that the large domain experiments are run for a longer period to allow the clouds to self-aggregate (this will be explained in greater detail in section 8).

### 3. Moisture control of cloud temperature

Changes in sea surface temperature result in shifts of the domain-averaged RCE temperature profile to warmer moist adiabats. The temperature profile shift is also accompanied by a shift in the cloud fraction profile. The FAT hypothesis suggests that changes between temperature profiles and cloud fraction profiles occur in lockstep. In other words, the cloud fraction profile, as a function of temperature, ought to remain fixed with changing sea surface temperature. To demonstrate the effect of sea surface temperature on cloud temperatures, the cloud fraction profiles for three different sea surface temperatures ( $28.5^\circ$ ,  $30.5^\circ$ , and  $32.5^\circ\text{C}$ ) are plotted as functions of temperature (Fig. 2). As in Kuang and

TABLE 1. List of experiments. Water vapor removal/addition refers to alterations to the water vapor concentration passed to the radiative transfer code. Note that all runs are performed for three different sea surface temperatures (28.5°, 30.5°, 32.5°C) except for experiments BREM and BADD (both done only at SST = 28.5°C; see section 8).

Name	Domain size	Resolution	Duration	Averaged days	Description
BASE	96 km × 96 km	1 km	100 days	50–100	No modification
REM	96 km × 96 km	1 km	100 days	50–100	Water vapor removal; $T_1 = 250$ K [see Eq. (2)]
ADD	96 km × 96 km	1 km	100 days	50–100	Water vapor addition; $T_1 = 250$ K; $T_2 = 220$ K; $K = 2$ [see Eq. (4)]
H2Oonly	96 km × 96 km	1 km	100 days	50–100	Zero out all radiatively active gases except water vapor
zeroO3	96 km × 96 km	1 km	100 days	50–100	Zero out only ozone
H2O+O3	96 km × 96 km	1 km	100 days	50–100	Zero out all radiatively active gases except water vapor and ozone
2xqv	96 km × 96 km	1 km	100 days	50–100	Doubled stratospheric water vapor
INVCLD	96 km × 96 km	1 km	100 days	50–100	Clouds invisible to radiative transfer model
2xLf	96 km × 96 km	1 km	100 days	50–100	Doubled latent heat of fusion
BIG	576 km × 576 km	3 km	125 days	75–125	Large domain, self-aggregated run
BREM	576 km × 576 km	3 km	75 days	25–75	As in REM except large domain, self-aggregated; initialized with end of BIG run so that self-aggregation has already taken place
BADD	576 km × 576 km	3 km	75 days	25–75	As in ADD except large domain, self-aggregated; initialized with end of BIG run

Hartmann (2007), we consider a grid cell to be cloudy if the nonprecipitating condensate concentration exceeds  $10^{-5}$  kg kg<sup>-1</sup>. The sea surface temperature was varied for each of the experiments listed in Table 1 (except for the BREM and BADD experiments discussed in Section 8).

Let us focus on the BASE experiments for a moment. BASE in this case refers to runs using the model-predicted water vapor for the radiative transfer calculations. As the surface temperature warms, a slight decrease in cloud fraction and a slight warming of the peak cloud fraction occur. A similar result was shown for GCMs by Zelinka and Hartmann (2010). They explained this change as being due to the large increase in static stability in the upper troposphere. We show in the next section that ozone heating, which is not a function of temperature, exerts a control on the stability. An increase in stability reduces the vertical gradient of diabatic vertical velocity—see Eq. (1). By mass continuity ( $\nabla_H \cdot \mathbf{v} + \partial\omega/\partial p = 0$ ), increased stability also weakens the horizontal mass convergence. For the REM and ADD cases, increasing sea surface temperature also decreases cloud fraction and causes the clouds to detrain at a slightly warmer temperature. These changes are smallest in the REM case since the maximum cloud fraction is lower and farther away from the influence of ozone heating.

We first demonstrate that we can change the temperature at which the cloud fraction peaks by changing the radiative cooling due to water vapor using the REM and ADD modifications described above by Eqs. (2) and (4), respectively. For the BASE, REM, and ADD cases,

the differences in cloud fraction profile as a function of temperature are striking (see Fig. 3). The water vapor removal (REM) shifts the peak cloud fraction (and hence, the anvil detrainment) to warmer ( $\sim 5^\circ\text{C}$ ) temperatures while the enhanced water vapor cooling likewise shifts the peak cloud fraction to colder temperatures. The above results suggest a strong connection between clear-sky radiative cooling due to water vapor and cloud-top temperature, as predicted by the FAT hypothesis. This connection is illustrated by computing the radiatively driven mass convergence for clear-sky conditions. We calculate mass convergence using Eq. (1). We expect that the clear-sky convergence profile caps the anvil cloud detrainment. That is, where we see a rapid decline in clear-sky convergence, we expect to see a coincident decline in cloud fraction (see Fig. 3).

Looking at the right-side panel of Fig. 3, the clear-sky convergence patterns show similar shifts to those of the cloud fraction in the left-side panel. Again, the enhanced water vapor (ADD) at upper levels is enough to shift the convergence profile to lower temperatures, while the reduced water vapor (REM) shifts the radiatively driven convergence profile to higher temperatures. It can be seen that the cloud fraction profile is capped by strong clear-sky convergence. Note that the maximum convergence does not line up with the maximum in cloud fraction. The level of maximum clear-sky convergence denotes the level of anvil detrainment. The maximum in cloud fraction is simply the level of largest cloud areal extent. Thin clouds, forming in situ or detraining from convective towers, have the largest areal extent.

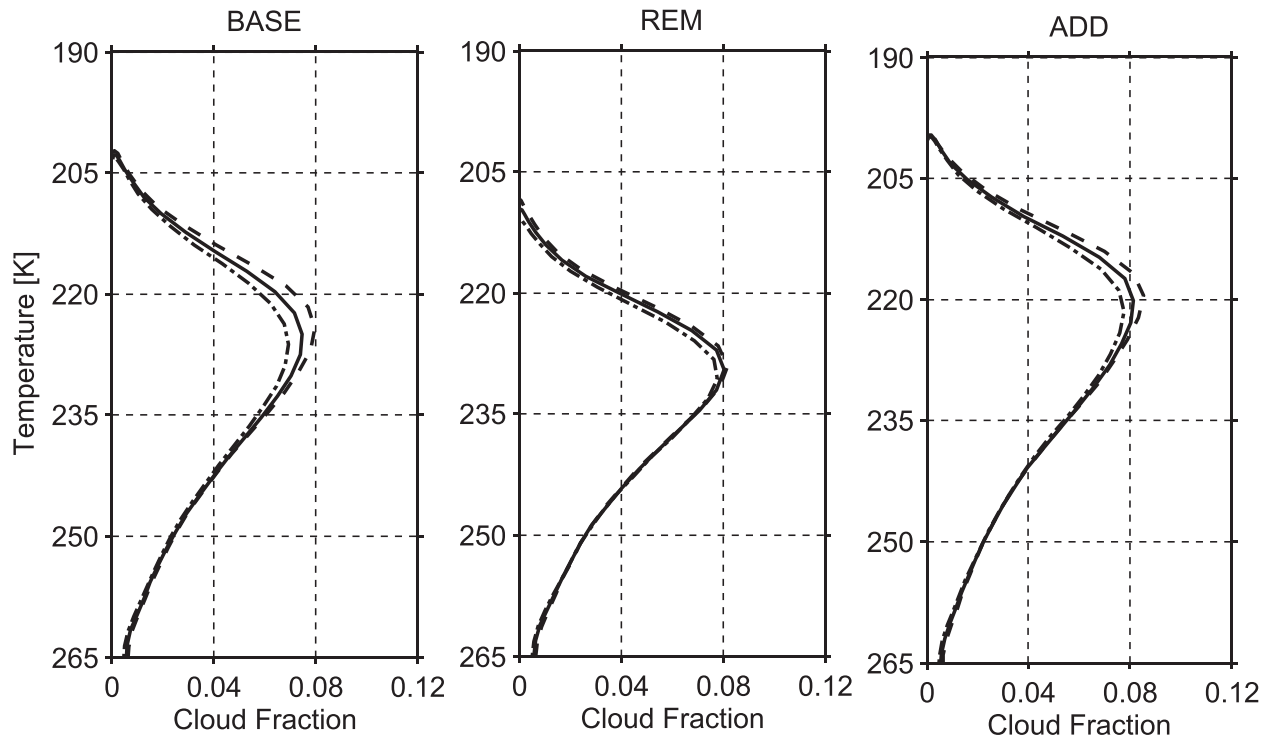


FIG. 2. Cloud fraction presented as functions of temperature. For each plot, lines show runs for SST = 28.5°C (dashed), SST = 30.5°C (solid), and SST = 32.5°C (dashed-dotted).

The convergence profiles exhibit similar shifts to warmer temperatures with increasing sea surface temperature (not shown) as do the cloud fraction profiles. The shift due to increasing sea surface temperature is not nearly as pronounced as that due to changes to the water vapor. Also, a slight decrease of maximum convergence strength with increasing sea surface temperatures occurs (not shown). The changes in convergence with sea surface temperature and the changes in cloud fraction with sea surface temperature are consistent with the PHAT hypothesis. Although we acknowledge that the cloud-top temperatures are not fixed with changing sea surface temperatures, the changes are small because the radiative cooling of water vapor still largely controls the anvil cloud-top temperatures. We demonstrate in section 4 that the small cloud warming with increasing sea surface temperature is associated with ozone heating, which is fixed to pressure levels in these experiments.

We return now to the role of stability in changes in cloud-top temperature (Chae and Sherwood 2010; Zelinka and Hartmann 2010). The stability profiles from the BASE, REM, and ADD experiments plotted as functions of height can be seen in Fig. 4. It can be seen that the large increase in static stability in the upper troposphere appears near the vertical level where the cloud fraction decreases. The stability increases slightly with

increasing sea surface temperature for each experiment (not shown).

For every case (BASE, REM, or ADD) and sea surface temperature, all of the stability profiles show a tremendous increase at temperatures colder than roughly 220 K ( $\sim 11$  km; see Fig. 4). To understand the behavior of stability it is helpful to consider its equation:

$$\sigma = -\frac{T}{\theta} \frac{\partial \theta}{\partial p} = -\frac{\partial T}{\partial p} + \frac{R_d T}{c_p p} = \frac{\Gamma - \Gamma_d}{\rho g}, \quad (6)$$

where  $R_d$  is the gas constant for dry air,  $c_p$  is the specific heat at constant pressure,  $\Gamma$  is the lapse rate,  $\Gamma_d$  is the dry adiabatic lapse rate,  $\rho$  is the density, and  $g$  is the acceleration due to gravity. The rapid increase with decreasing temperature is partly a result of the use of a pressure coordinate system. In height coordinates, the stability is simply the difference between the actual lapse rate  $\Gamma$  and the dry adiabatic lapse rate  $\Gamma_d$ . Clouds occur where radiative cooling can keep the lapse rate close to the adiabatic lapse rate. We consider in detail what controls the stability of the upper troposphere in our model as well as the real atmosphere. For example, changes in dynamics or radiatively active gases other than water vapor may play a role in the stability of the upper troposphere. Ozone heating in the upper troposphere

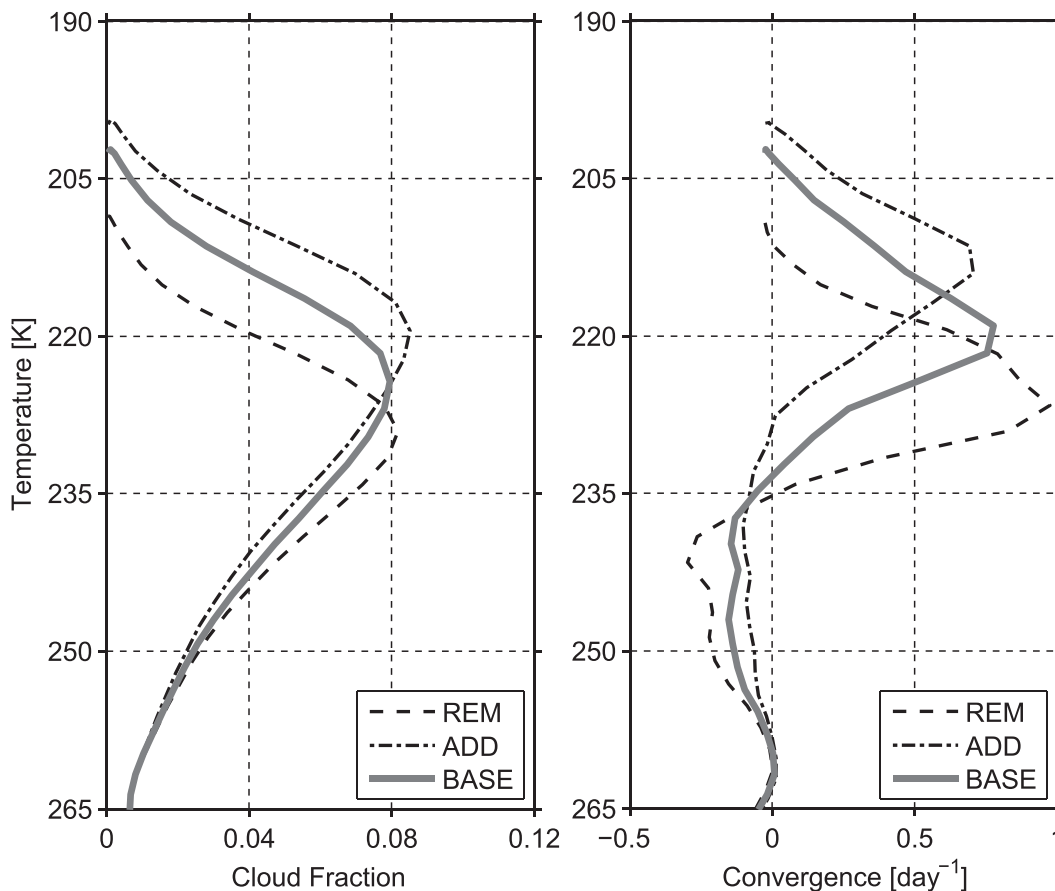


FIG. 3. Cloud fraction and clear-sky convergence shown for the BASE (solid), REM (dashed), and ADD (dashed-dotted) runs. All plots show SST = 28.5°C.

increasingly drives a more stable lapse rate. Kuang and Hartmann (2007) have already demonstrated that an imposed large-scale vertical velocity of  $0.3 \text{ mm s}^{-1}$  is capable of weakening the stratification at heights above the 220-K temperature level and cooling the anvil cloud-top temperature by roughly 1 K. In the same study, Kuang and Hartmann (2007) also doubled the carbon dioxide concentrations and found no significant change to the clouds. We perform additional experiments (outlined in Table 1) to expose the impacts of the radiatively active gases other than water vapor.

#### 4. The role of ozone, carbon dioxide, and stratospheric water vapor

To investigate the role of gases other than water vapor in controlling upper-tropospheric stability, we change the concentrations of those gases within the model. The RRTM radiation scheme specifies nine additional active gases beyond water vapor: ozone, carbon dioxide, methane, nitrous oxide, oxygen, chlorofluorocarbon 11 (CFC-11), CFC-12, CFC-22, and carbon tetrachloride (CCL-4).

In all simulations, all CFC and CCL concentrations are set to zero. Water vapor is the only dynamic variable; that is, all of the other gas concentrations are fixed in space and time for all experiments. We make three distinct modifications to the radiatively active trace gases and perform each of these experiments with the same three sea surface temperatures used above. The three experiments—also described in Table 1—are the following: H2Oonly, where all radiatively active gas concentrations are zero except water vapor; zeroO3, ozone concentrations set to zero; and H2O + O3, zero out all radiatively active gases except water vapor and ozone. The design of these experiments is meant to separate the relative contributions to the clear-sky convergence and cloud profiles from ozone and carbon dioxide, which are believed to have the strongest influences other than water vapor. Figure 5 shows the responses of cloud fraction and clear-sky convergence profiles to changing the radiatively active gases.

We use the standard RRTM ozone profile. We note the RRTM upper-tropospheric ozone concentrations are higher than those found in ozonesonde data from the tropics (Kley et al. 1996; Lawrence et al. 1999; Thompson

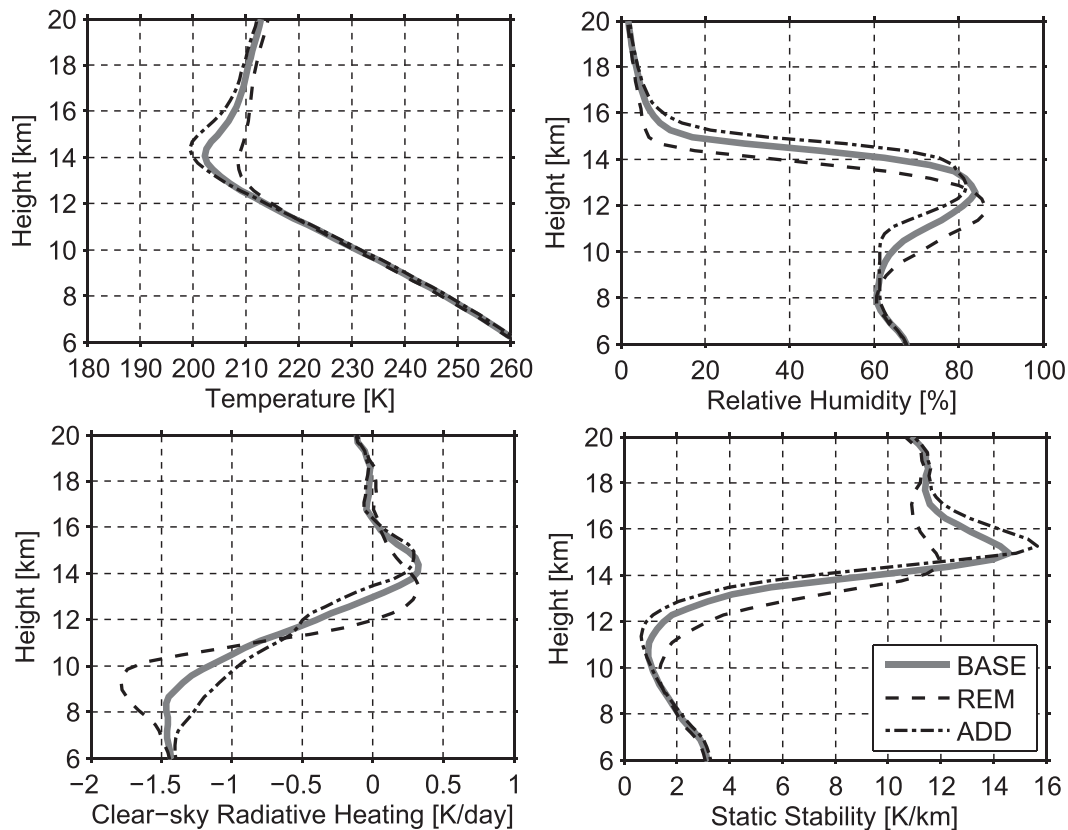


FIG. 4. Temperature, relative humidity (with respect to ice; using model-predicted water vapor for all three experiments), clear-sky radiative heating, and static stability profiles shown as functions of height for BASE (solid), REM (dashed), and ADD (dashed-dotted). All profiles show SST = 28.5°C.

et al. 2011). As an additional sensitivity test, we construct a new ozone profile using ozonesonde data from Fiji that is part of the Southern Hemisphere Additional Ozonesondes (SHADOZ) program (Thompson et al. 2003). The ozone profile is constructed as the mean of eight profiles, that sampled both the troposphere and stratosphere, taken on the following dates: 10 February, 16 March, 30 March, 14 April, 16 June, 27 June, 13 July, and 5 August, all during 2011. The RRTM ozone profile has higher ozone concentrations in the whole of the troposphere (on the order of several parts per billion), but especially in the range of 100–200 mb (on the order of hundreds of parts per billion), the region of most concern. We find that the clouds detrain at colder temperatures and have more areal extent in the simulations with the lower ozone concentrations from the SHADOZ data. This is consistent with the hypothesis that ozone heating drives a stable lapse rate that limits convection. The clouds still detrain at warmer temperatures when the sea surface temperature is increased even with the tropical ozone profile, but the magnitude of the warming is less than in the BASE simulations ( $\sim 0.29$  K between 28.5° and 32.5°C

for BASE compared to  $\sim 0.20$  K, for the tropical ozone simulations).

In the H2Oonly experiment, water vapor is the only radiatively active gas in the model. Without ozone and carbon dioxide, we expect a pure FAT response from the clouds. Figure 6 shows that indeed the cloud fraction profiles show almost no response to varying sea surface temperature when water vapor is the only radiatively active gas. This insensitivity suggests that ozone or carbon dioxide contribute significantly to the warming trend of cloud tops with increasing SST in the BASE, REM, and ADD experiments.

Comparing the zeroO3 and BASE experiments shows the effect of ozone heating on warming the clouds and reducing cloud fraction. The convergence profile suggests ozone heating reduces the radiatively driven convergence in the upper troposphere (see Fig. 5). The same shift of the clouds to cooler temperatures is seen in both experiments where ozone is removed: H2Oonly and zeroO3. In this model, ozone is specified as a function of pressure. Ozone heating increases the stability in the upper troposphere, making the stability a function of

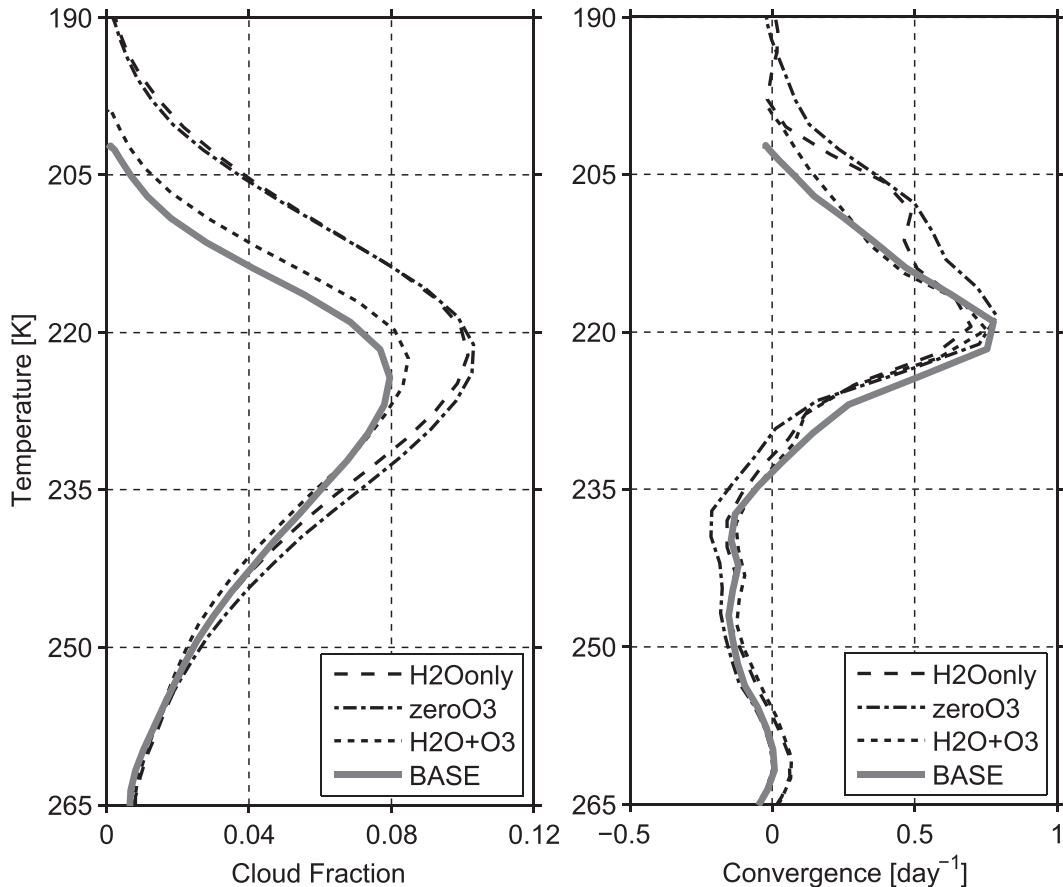


FIG. 5. Cloud fraction and clear-sky convergence shown for H<sub>2</sub>Oonly (dashed), zeroO<sub>3</sub> (dashed-dotted), H<sub>2</sub>O+O<sub>3</sub> (dotted), and BASE (solid) runs. All plots show SST = 28.5°C.

temperature and pressure where ozone heating is strong. The pressure dependence of stability inhibits clouds from ascending as high as they would under a pure FAT scenario, leading to cloud detrainment occurring at slightly warmer temperatures as the SST warms. In the real atmosphere the ozone profile is not fixed. As the tropical troposphere warms and expands, it is reasonable to think that the ozone concentrations will be reduced at the pressure levels that become part of the well-mixed troposphere. Ozone destruction could reduce the warming of cloud-top temperatures in the warmest sea surface temperature runs. Kuang and Hartmann (2007) investigated the impacts of shifting the ozone profile vertically. They observed a change in the clouds only for shifts downward, which were deemed unrealistic for the actual tropics. They observed no change for a shift of the profile upward. In our experiments, removing ozone allows the cloud to rise to lower pressures nearly isothermally as the sea surface temperature increases.

The H<sub>2</sub>O + O<sub>3</sub> experiment further demonstrates the effect of ozone. The inclusion of ozone is sufficient to

create the slight warming of clouds with increasing sea surface temperature. Assuming the radiative effects of nitrous oxide, oxygen, and methane are small, the H<sub>2</sub>O + O<sub>3</sub> case also gives some insight into the effect of carbon dioxide in our simulations. Figure 5 shows that carbon dioxide warms the clouds. More specifically, Fig. 7 shows that the presence of carbon dioxide keeps the cold point from getting as cold as when carbon dioxide is removed (cf. BASE with H<sub>2</sub>O + O<sub>3</sub>). Thus, the upper troposphere is actually less stable without carbon dioxide than with it. This interpretation is consistent with the increase in radiatively driven convergence at higher altitudes when carbon dioxide is removed. The decrease in stability allows the clouds to rise to colder temperatures. While the upper troposphere is colder, the stratosphere is substantially warmer without carbon dioxide present as expected.

Stratospheric water vapor concentrations are largely controlled by the cold point temperature and methane chemistry (Solomon et al. 2010). The cold point temperature is sensitive to sea surface temperature, ozone, and large-scale ascent (Oman et al. 2008) as well as convection

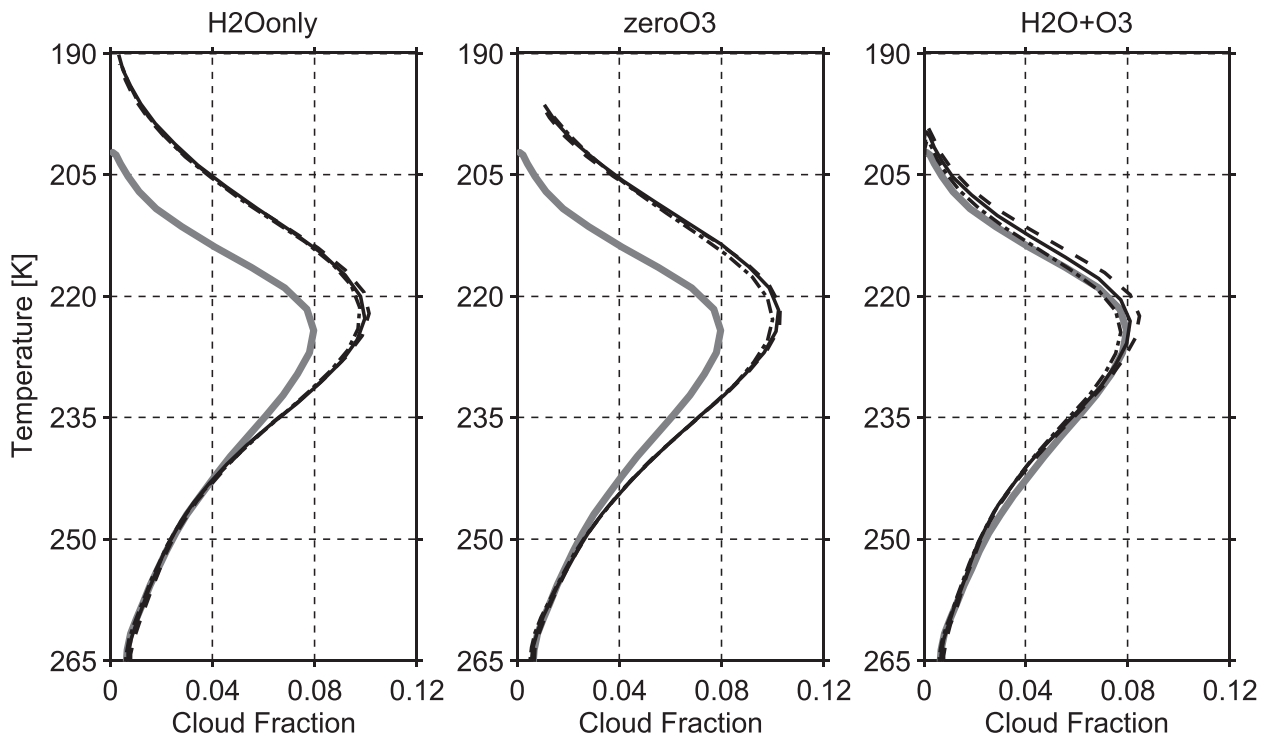


FIG. 6. Cloud fraction presented as functions of temperature. For each plot, lines show runs for SST = 28.5°C (dashed), SST = 30.5°C (solid), and SST = 32.5°C (dashed–dotted). BASE, SST = 28.5°C (gray, solid) is shown for comparison.

(Kuang and Bretherton 2004). Because our model does not include a Brewer–Dobson circulation or methane chemistry, we cannot accurately predict the stratospheric water vapor value, so fixing its concentration for these experiments is necessary. As a simple test of the role of stratospheric water vapor, we double its concentration to 7 ppmv. Clouds in the 2xqv experiment detrain at a slightly warmer temperature than the BASE experiment (not shown). Kuang and Hartmann (2007) also performed a doubled stratospheric water vapor experiment (using a different radiative transfer code than we use). Their results show a similar slight warming of the clouds due to the increased water vapor.

### 5. Radiative effects of cloud

We next investigate the clouds' radiative impact on their own evolution in our model. To do this, we remove the effect of cloud on radiative transfer. In the INVCLD simulations, the clear-sky flux and heating rate calculations are used to compute the tendencies for liquid water/ice moist static energy—the model's prognostic energy quantity. In other words, the clouds do not contribute to the radiative heating in the model. If the detrainment level of the clouds does not align with the clear-sky convergence level when the clouds are invisible, then the

radiative interaction of the clouds must be an important factor in determining that level. Again, we specify the same three sea surface temperatures for this experiment and examine the temperature profiles of the cloud fraction and clear-sky convergence. We find that the cloud levels remain consistent with that of the clear-sky convergence. Also, the cloud-top temperatures for the INVCLD are similar to those of the BASE experiments. Two possible explanations for the insensitivity of the cloud-top temperature to radiative effects of clouds immediately come to mind. First, clouds only appear where clear-sky radiative convergence drives cloud formation, so clouds cannot change their detrainment level. Second, whatever radiative impact clouds may have is being canceled by something else. McFarlane et al. (2007) have shown that clouds have nonnegligible heating rates in the upper troposphere and it is reasonable to expect that these heating rates influence the clear-sky region. In the model, clear-sky cooling increases when the radiative effects of clouds are eliminated, seen in Fig. 8. This additional cooling, however, is balanced by a strengthening of stability, which results in the convergence, and hence the clouds, remaining at the same level. It is perhaps not surprising that the clouds have little effect on their detrainment temperature in this model simply because the cloud fraction is small. The total cloud cover of clouds with tops colder

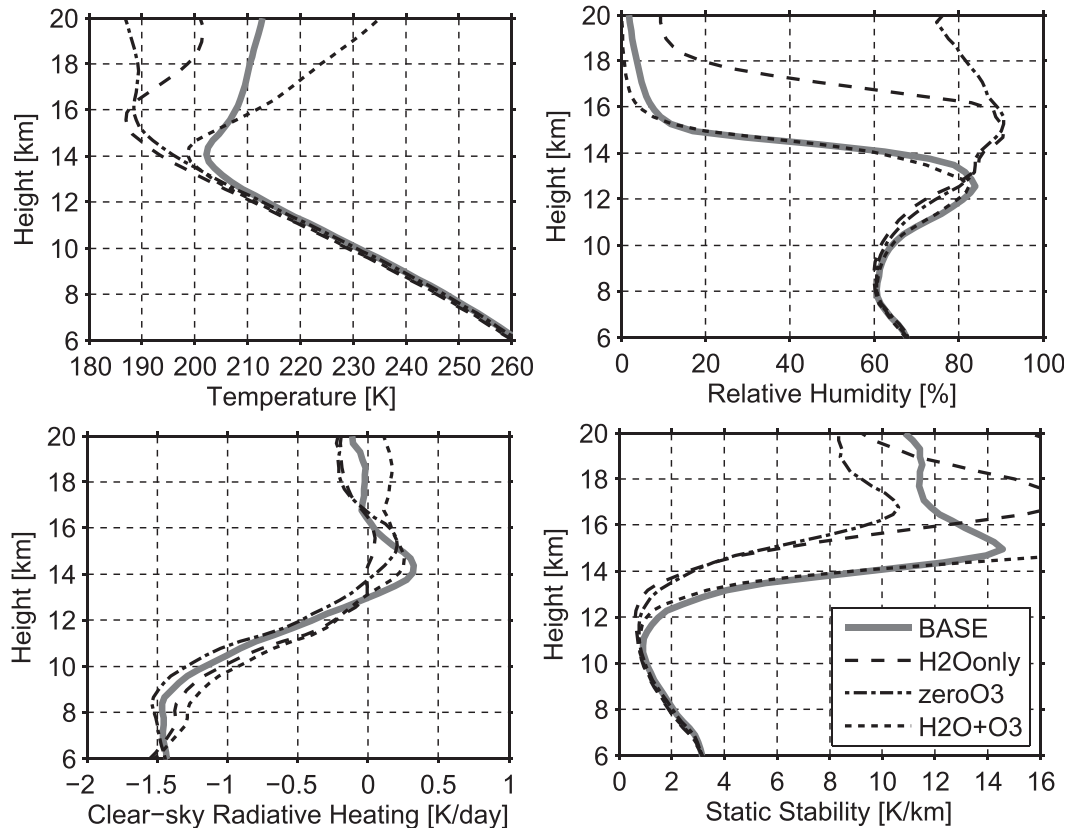


FIG. 7. Temperature, relative humidity (with respect to ice), clear-sky radiative heating, and static stability profiles shown as functions of height for BASE (solid), H2Oonly (dashed), zeroO3 (dashed-dotted), and H2O+O3 (dotted) runs. All profiles show SST = 28.5°C.

than 265 K is about 0.12 for the BASE experiment with SST = 28.5°C. High cloud (tops higher than 440 mb) fraction is roughly 40%–50% in convective regions estimated from MODIS satellite retrievals (Hong et al. 2007).

The cloud fraction for the INVCLD experiment decreases compared to the BASE experiment. To investigate this effect further, we split the cloud fraction into three optical depth ( $\tau$ ) categories as in Kubar et al. (2007): thin ( $\tau < 4$ ), anvil ( $4 < \tau < 32$ ), and thick ( $\tau > 32$ ). Looking at Fig. 9 it is apparent that the INVCLD experiment has fewer thin clouds than the BASE experiment. The thick and anvil cloud fractions are greater for the INVCLD experiments, suggesting something is inhibiting the clouds from spreading and thinning out. Garrett et al. (2005) proposed absorption of thermal radiation at cloud base and emission at cloud top spread anvil cirrus by creating density currents in the cloud. The spread they calculated using this method matched the Cirrus Regional Study of Tropical Anvils and Cirrus Layers–Florida Area Cirrus Experiment (CRYSTAL-FACE) observations (Garrett et al. 2005). Cirrus were shown to spread in a cloud-resolving model

because of thermal radiation absorption at cloud base and emission at cloud top (Krueger and Zulauf 2005; Garrett et al. 2006). Tropical tropopause layer (TTL) cirrus have been shown to self-maintain themselves through radiative interactions (Durrán et al. 2009; Dinh et al. 2010). Durrán et al. (2009) showed that the radiative heating of thin TTL cirrus causes them to rise, and the resulting circulation, pulling air in toward the bottom and pushing air out toward the top, spreads the cloud. In the INVCLD experiment, we remove the heating and cooling for the cloud and thus remove the mechanisms for forming (Garrett et al. 2005) and maintaining (Durrán et al. 2009) a larger fractional coverage of thin cirrus. Although our model has coarser resolution than the models used by Garrett et al. (2005) or Durrán et al. (2009), their results are in agreement with those from our INVCLD experiment.

## 6. Cloud-weighted temperature

We quantify the changes in the profiles by determining the cloud-weighted and convergence-weighted temperatures. This is done similar to Kubar et al. (2007):

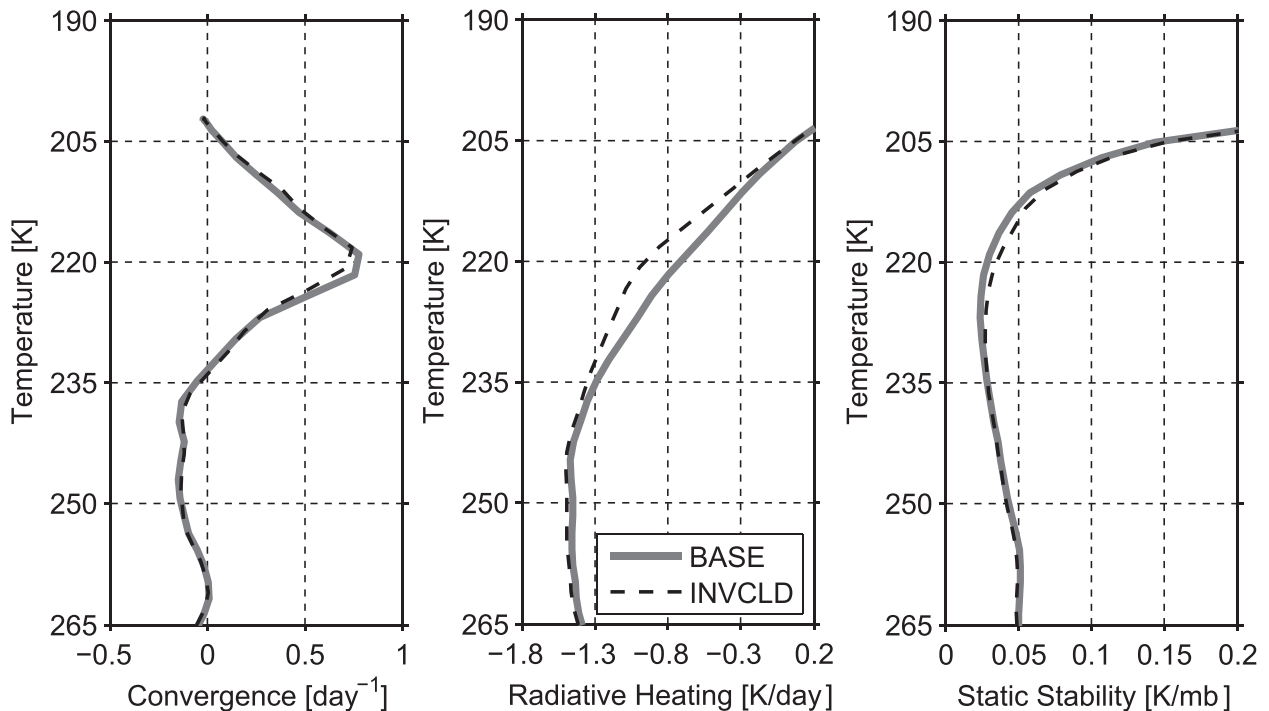


FIG. 8. BASE (solid, gray) and INVCLD (dashed, black) profiles for (left) clear-sky convergence, (middle) clear-sky radiative heating, (right) static stability. All plots show SST = 28.5°C.

$$T_c = \frac{\int_{T_{cp}}^{245K} C \times T dT}{\int_{T_{cp}}^{245K} C dT}. \quad (7)$$

Here,  $C$  is replaced with either the convergence or cloud fraction profile and  $T_{cp}$  is the cold point tropopause temperature. The upper limit is arbitrary. We select

245 K because it corresponds roughly to the level where longwave cooling begins to decline toward zero in our model.

The cloud-fraction-weighted temperatures are plotted with respect to their corresponding convergence-weighted temperatures in Fig. 10. The weighted temperature captures more than just the cloud tops, since the cloud fraction is weighted lower in the cloud and clear-sky convergence marks the top of the well-mixed convective

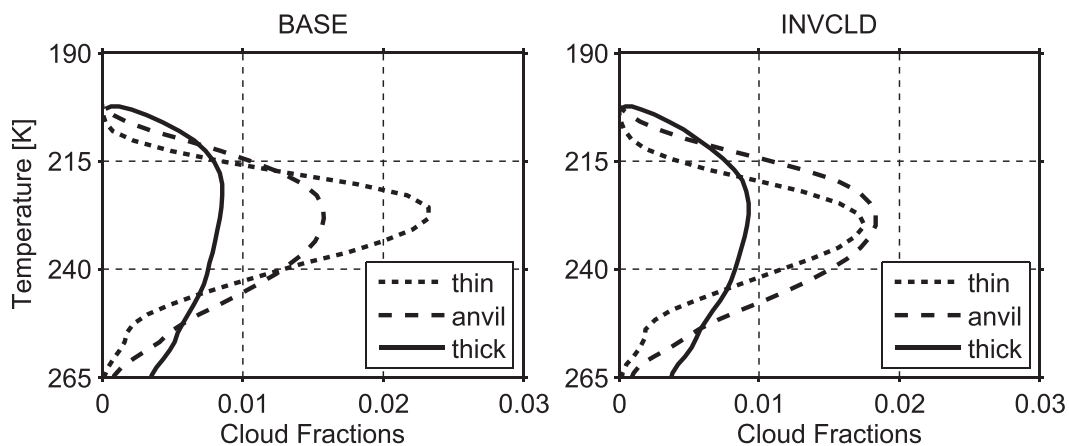


FIG. 9. Cloud fraction separated by optical depth bins: thin ( $\tau < 4$ ), anvil ( $4 < \tau < 32$ ), and thick ( $\tau > 32$ ). Both plots show SST = 28.5°C.

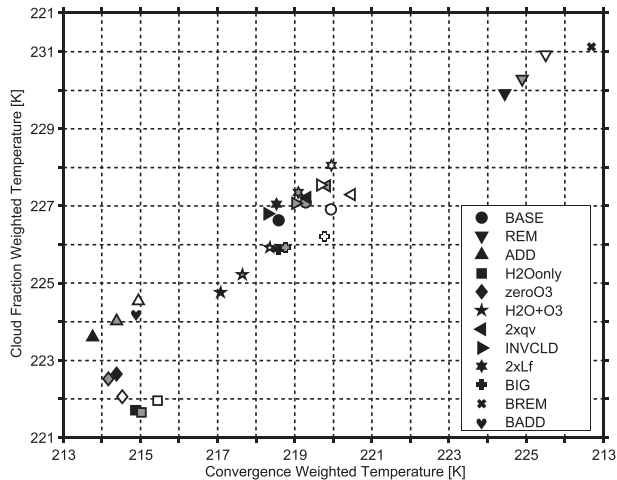


FIG. 10. Convergence-weighted temperature on the x axis; cloud fraction-weighted temperature on y axis. For all symbols, the shading corresponds to SST = 28.5°C (black), SST = 30.5°C (gray), SST = 32.5°C (white).

layer and the beginning of the TTL. Thus, it should not be expected that  $T_{\text{conv}} = T_{\text{clid}}$ . Nonetheless, we expect that convergence-weighted and cloud-fraction-weighted temperatures will change in parallel. For example, increases (decreases) in water vapor's ability to cool the atmosphere lead to lower (higher) weighted temperatures. Figure 10 shows warming of the clouds with increasing sea surface temperature for all of the experiments with ozone, and unchanging cloud temperatures with increasing SST for those experiments without ozone. For example, the H2Oonly case varies the least for both convergence- and cloud-weighted temperature ( $<0.5^{\circ}\text{C}$ ) while the cases with ozone vary by about  $2^{\circ}\text{C}$  for a  $4^{\circ}\text{C}$  change in SST.

Table 2 shows the differences in the weighted temperatures between SST = 32.5°C and SST = 28.5°C for each experiment. The increase in convergence-weighted and cloud-weighted temperatures are smallest for the experiments without ozone and in the case with doubled stratospheric water vapor. BASE has a small change in cloud-weighted temperature as well. The final column of Table 2 shows the change in the temperature where the domain-mean cloud fraction is highest (for high cloud only). Table 2 shows an increase in temperature of the cloud fraction peak of about 1.5–2 K for all experiments except H2Oonly and BIG.

We next address whether there is statistical significance of the differences between cloud fraction profiles for different sea surface temperatures. The model output cloud fraction profiles are averaged over 2.5 days. The autocorrelation of each 2.5-day mean is used to get the effective number of degrees of freedom following Bretherton et al. (1999). A  $t$  statistic is then used to attribute significance at the 95% level. For most experiments, a  $4^{\circ}$  change in

TABLE 2. Difference in cloud-weighted temperature ( $\Delta T_{\text{clid}}$ ), convergence-weighted temperature ( $\Delta T_{\text{conv}}$ ), and temperature of the cloud fraction peak (Peak  $C_T$ ) between SST = 32.5°C and SST = 28.5°C.

Experiment	$\Delta T_{\text{clid}}$	$\Delta T_{\text{conv}}$	Peak $C_T$
BASE	0.29	1.36	1.98
REM	1.00	1.07	1.53
ADD	0.93	1.19	2.03
H2Oonly	0.26	0.58	-0.81
zeroO3	-0.59	0.15	1.72
H2O+O3	1.17	1.27	1.98
2xqv	0.09	1.15	1.82
INVCLD	0.74	1.36	1.66
2xLf	1.01	1.42	1.97
BIG	0.33	1.20	-1.41

SST creates a significant difference in cloud fraction, while a  $2^{\circ}$  change in SST does not (not shown). The experiments that show no difference for all three sea surface temperatures are those without ozone (H2Oonly and zeroO3), 2xqv, and BIG. The upper-tropospheric cloud temperatures are invariant to sea surface temperature when ozone is not present in the simulation, as expected.

## 7. Latent heating

So far we have limited the discussion to changes in the radiative heating caused by changes in concentrations of radiatively active gases and the radiative effects of clouds. We now test whether we can change the cloud temperature by modifying the latent energy available to raise parcels. Condensational heating decreases with the saturation vapor pressure in the cold upper troposphere. By giving parcels greater energy, we test whether a drop off in condensational heating controls cloud-top temperature, rather than the radiative relaxation.

In the 2xLf experiments, everything is identical to the BASE experiments except that we double the latent heat of fusion. The cloud profile does not shift to colder temperatures. In fact, it shifts to slightly warmer temperatures, as compared to BASE, mostly because the cloud fraction decreases in the upper troposphere (not shown). The same increase in cloud-top temperature with increasing sea surface temperature is seen with the 2xLf experiment (Fig. 11). Moreover, static stability increases compared to the BASE runs resulting from the greater release of latent heat per unit of condensation. This causes the radiatively driven convergence to decrease and its profile to shift toward warmer temperatures (not shown), leading to warmer anvil tops with lower fractional cloud cover. Thus, a decrease in latent heating as the air becomes colder higher up in the troposphere

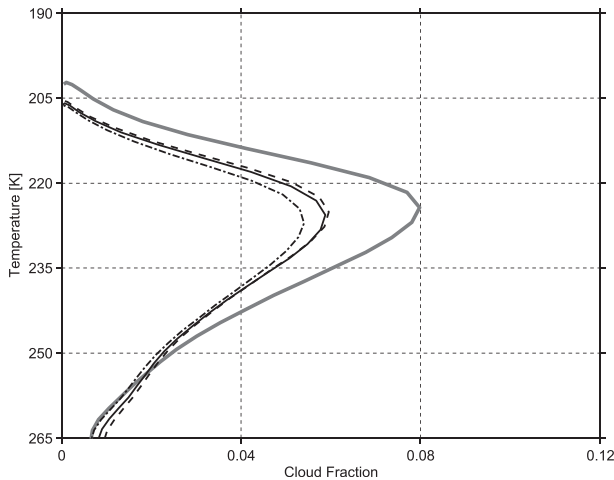


FIG. 11. Cloud fraction presented as functions of temperature for 2xLf case. Lines show runs for SST = 28.5°C (dashed), SST = 30.5°C (solid), and SST = 32.5°C (dashed-dotted). BASE, SST = 28.5°C (gray, solid) is shown for comparison.

does not seem to be the reason that anvil clouds have a nearly constant temperature in these simulations. The invariance of the detrainment temperature of the clouds to the latent heat of fusion is consistent with the notion that cooling by radiative emission to maintain a convectively favorable environment is the primary control of cloud temperature in the tropical upper troposphere.

## 8. Self-aggregation of clouds

We have relied on the conceptual model of a dynamic circulation between the clear- and cloudy-sky regions as described by Hartmann and Larson (2002), yet the small model domain with its random, “popcorn” convection pattern does not show a well-organized circulation pattern. We can create an organized circulation in the model if we allow self-aggregation of the clouds to occur. It has been shown in models that RCE can be maintained while cumulus convection self-aggregates or bunches together in the domain (Held et al. 1993; Bretherton et al. 2005). The process of self-aggregation causes the domain to shift to a higher moist adiabat (than in the unaggregated case) because of the higher moist static energy air in the boundary layer of the convective region as shown by Bretherton et al. (2005). Self-aggregation also causes a drying of the nonconvective region. One might expect that this drying could have a similar effect to the REM experiment. Held et al. (1993) explained self-aggregation through the memory convection leaves in the moisture field, in which future convection rises more easily where midtropospheric moisture is higher. The self-aggregation anomaly is sensitive to a number of factors [many of which

are outlined by Bretherton et al. (2005)]. For example, changing domain size and resolution is sufficient to determine whether self-aggregation occurs. Self-aggregation does not occur in the SAM model with the 96 km  $\times$  96 km domain and 1-km resolution. Following Bretherton et al. (2005), we achieve self-aggregation using a domain size of 576 km  $\times$  576 km with 3-km resolution. Self-aggregation has direct parallels to the intertropical convergence zone (ITCZ), in that a large-scale circulation occurs between the clear- and cloudy-sky regions with subsidence in the clear-sky region and rising motion in the cloudy-sky region.

The self-aggregation process occurs during model spinup, but requires a longer spinup time (75 days) than the small domain experiments (50 days) shown in previous sections (see Table 1). With self-aggregation occurring in the model, we apply the same removing and adding of water vapor [see Eqs. (2) and (4), respectively]. To save computation time, the modification experiments—BREM and BADD (the same as REM and ADD, respectively, but for an aggregated cloud field)—are initialized with the end of the BIG experiment such that the clouds are already aggregated. The adjustment to a new radiative-convective equilibrium profile takes 25 days. The model is run an additional 50 days for the statistical profiles shown.

Self-aggregation causes the clouds to rise to higher altitudes. The domain-mean cloud fraction, however, is smaller for the self-aggregated experiments compared to the nonaggregated ones. While the BIG experiments with sea surface temperatures of 30.5° and 32.5°C showed the same near constancy of cloud-weighted temperature with SST as the BASE case (Fig. 10), the cloud fraction profiles do not show an increase of cloud-top temperature for increasing SST (see Fig. 12). The increase in cloud-weighted temperature is due to an increase in midlevel clouds, relative to the peak amount, which biases the weighted temperature value. The BREM and BADD experiments behave like the REM and ADD experiments: the clouds detrain at warmer temperatures in the BREM experiments and colder temperatures in the BADD experiment.

We also examine the humidity profiles between the moist and dry regions to see if there is any evidence that the drying of the clear-sky region is influencing the cloud temperature. To sample the wet and dry regions, we divide the domain into a 16  $\times$  16 horizontal grid and take the wettest and driest quartiles of that grid. Here, “wettest” and “driest” are the highest and lowest mean water vapor paths, respectively. Though the dry region has substantially less water vapor in the midtroposphere, the water vapor profiles of the wet and dry regions converge in the upper troposphere (not shown). The uniform upper-level humidity suggests that detrainment

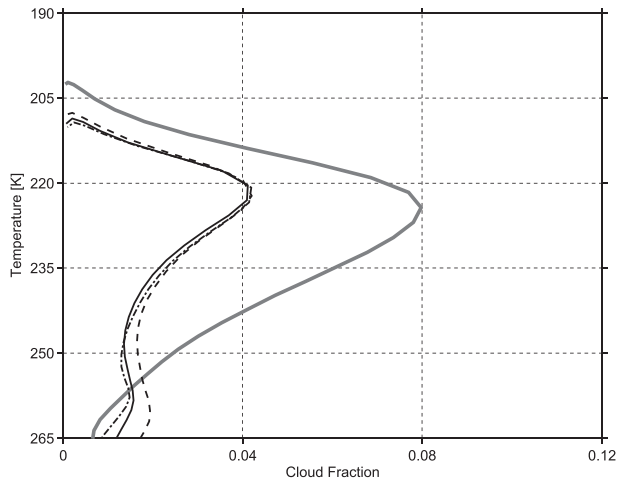


FIG. 12. Cloud fraction presented as functions of temperature for the BIG case. Lines show runs for SST = 28.5°C (dashed), SST = 30.5°C (solid), and SST = 32.5°C (dashed-dotted). BASE, SST = 28.5°C (gray, solid) is shown for comparison.

and advection of water from the convective region covers the entire domain. Water vapor advected to the clear-sky region allows for stronger cooling in the upper troposphere. The temperature and stability profiles in the clear and convective regions are identical because of gravity waves (“convective adjustment”).

Figure 13 shows the mass fluxes (calculated simply as the product of vertical velocity and density for each grid space) for the BIG experiments compared with BASE. Mass fluxes are averaged over cloudy columns as well as the unsaturated environment (the mass fluxes are equal and opposite by construction since no mass leaves or enters the model domain). A cloudy column is one such that the column-averaged cloud (water + ice) amount surpasses  $5 \times 10^{-4} \text{ kg kg}^{-1}$  (roughly twice the domain-averaged column amount). While the mass flux in the middle troposphere is less in the self-aggregated experiment compared to BASE, it is greater in the upper troposphere near the cold point tropopause. Less mass flux shows that the organized large-scale circulation (with the updrafts grouped together and subsidence region surrounding them) in the aggregated cloud field is weaker than the mesoscale circulations (the unorganized updraft and subsidence regions in the small domain simulations) created in the nonaggregated experiments. Changing the threshold used for determining the cloudy skies did not qualitatively alter the results. The local maximum in mass flux at  $\sim 10 \text{ km}$  in the BASE case suggests a secondary circulation. For the mass flux to increase with altitude, the vertical velocity must also increase with altitude—since density decreases. An increasing vertical velocity suggests convergence in the horizontal (note that this convergence

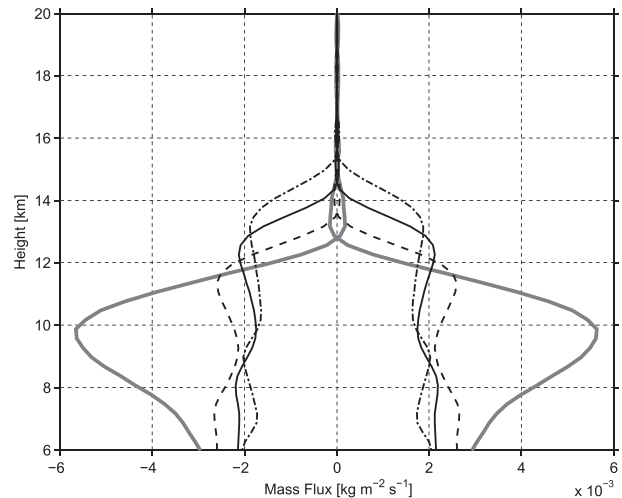


FIG. 13. Mass fluxes for cloudy (positive) and unsaturated environment (negative) presented as functions of height for BIG case. Lines show runs for SST = 28.5°C (dashed), SST = 30.5°C (solid), and SST = 32.5°C (dashed-dotted). BASE, SST = 28.5°C (gray, solid) is shown for comparison.

is in the cloudy sky and is below the level of anvil detrainment). The BIG mass flux profiles suggest that convection regularly approaches the height of the cold point when aggregated (14, 15, and 16 km for SST = 28.5°, 30.5°, and 32.5°C, respectively). Overshooting convection can warm the cold point by mixing down high potential energy air. The cold point temperature is 5 K warmer in the BIG experiment than for the BASE experiment. The warmer upper-tropospheric temperatures in the aggregated experiment allow for greater water vapor cooling. Stronger water vapor cooling cancels the ozone warming to make the clouds rise isothermally in our aggregated experiments in response to SST increases.

## 9. Conclusions

The sensitivity of tropical cloud-top temperature to radiative cooling by water vapor is tested using the SAM 3D cloud-resolving model. We demonstrate that changes in the ability of water vapor to cool the air have a direct influence on the cloud-top temperature. Weakened cooling increases cloud-top temperatures, and strengthened cooling decreases cloud-top temperatures. These results agree with expectations from the Fixed Anvil Temperature (FAT) hypothesis proposed by Hartmann and Larson (2002) as well as model results from Kuang and Hartmann (2007) and observations by Kubar et al. (2007). Cloud-top temperature is shown to be nearly insensitive to sea surface temperature. A slight warming of the clouds is shown for increasing sea surface temperatures, attributed to an increase in static stability in the

upper troposphere [which agrees with observations from Chae and Sherwood (2010) as well as an analysis of GCM results by Zelinka and Hartmann (2010)]. A slight decrease of cloud fraction is also shown for increasing sea surface temperatures. The responses to sea surface temperature changes are minor compared to those due to changes in radiative cooling by water vapor, suggesting water vapor cooling controls the cloud-top temperature. This produces a positive longwave cloud feedback since cloud emission temperature remains roughly constant as the surface warms.

The radiative impacts of ozone, carbon dioxide, and the clouds are shown to be secondary to that of water vapor. The simulations with and without ozone suggest that the stability increase caused by radiative heating of ozone causes the slight warming of the clouds observed with increasing sea surface temperature. Carbon dioxide increases the stability of the upper troposphere, causing clouds to detrain at warmer temperatures. Cloud radiative heating has little effect on determining the temperature of anvil detrainment in our experiments. While the rapid decline with height in water vapor in the upper troposphere is shown to have the strongest influence on the heating and stability profile, stratospheric water vapor plays a nontrivial role in determining the heating profile as well as the stability of the upper tropical troposphere.

Further experiments test if declining condensational heating is a strong constraint on cloud-top temperature. Doubling the latent heat of fusion stabilizes the uppermost layers of the troposphere, inhibiting convection from reaching temperatures as cold as those seen in the BASE simulations, and reducing the high cloud amount. With a large domain, convection is able to self-aggregate, but the weak sensitivity of cloud temperatures to surface temperature is very similar to that of the unaggregated cases. In the presence of an organized circulation, such as that caused by the simulation reaching a state of self-aggregation, the same control of cloud-top temperature by emission from water vapor remains. In fact, convective organization creates a stronger coupling of the clear- and cloudy-sky regions keeping the clouds at a fixed temperature. The circulation's effect on the clouds is stronger than the small heating because of fixed ozone seen in the unaggregated experiments.

For our simulations, changing sea surface temperature warms the clouds because the ozone profile is a fixed function of pressure. A fixed ozone profile is probably not a realistic feature of the tropics. The effect of ozone may change as the troposphere warms and expands and vertical mixing reduces ozone concentrations at pressure levels that become part of the well-mixed troposphere (Kley et al. 1996). The simulations using the ozone profile constructed from SHADOZ data also show that

lowering upper-tropospheric ozone concentrations causes the clouds to detrain at colder temperatures. Increasing stratospheric water vapor increases the cloud-top temperature in our simulations. Stratospheric water vapor (as measured by balloon over Boulder, Colorado) has increased since 1980 (Hurst et al. 2011). However, the increase is not monotonic and there are multiple periods of decrease in the record. Our model does not include any supradomain-scale (outside of the domain of the simulation) circulation, but we know that adiabatic processes can influence the stability as well as the cold point tropopause temperature. In addition, large-scale motions can change the humidity profile of the atmosphere, and thus, the radiative cooling profile. Quantifying the effects of factors beyond our RCE model to the clear-sky convergence will be important for determining the energy budget of the tropics.

*Acknowledgments.* The authors wish to thank Peter Blossey for his help running the SAM cloud-resolving model, as well as Thomas Ackerman and Christopher Bretherton for helpful discussions. The authors also thank Zhiming Kuang and the other reviewers for their comments. The work was supported by the Atmospheric and Geospace Sciences Division of the National Science Foundation Grant AGS-0960497.

#### REFERENCES

- Bretherton, C. S., M. Widmann, V. P. Dymnikov, J. M. Wallace, and I. Blade, 1999: The effective number of spatial degrees of freedom of a time-varying field. *J. Climate*, **12**, 1990–2009.
- , P. N. Blossey, and M. Khairoutdinov, 2005: An energy-balance analysis of deep convective self-aggregation above uniform SST. *J. Atmos. Sci.*, **62**, 4273–4292.
- Chae, J. H., and S. C. Sherwood, 2010: Insights into cloud-top height and dynamics from the seasonal cycle of cloud-top heights observed by MISR in the west Pacific region. *J. Atmos. Sci.*, **67**, 248–261.
- Dinh, T. P., D. R. Durran, and T. P. Ackerman, 2010: Maintenance of tropical tropopause layer cirrus. *J. Geophys. Res.*, **115**, D02104, doi:10.1029/2009JD012735.
- Durran, D. R., T. Dinh, M. Ammerman, and T. Ackerman, 2009: The mesoscale dynamics of thin tropical tropopause cirrus. *J. Atmos. Sci.*, **66**, 2859–2873.
- Eitzen, Z. A., K. Xu, and T. Wong, 2009: Cloud and radiative characteristics of tropical deep convective systems in extended cloud objects from CERES observations. *J. Climate*, **22**, 5983–6000.
- Eyring, V., and Coauthors, 2006: Assessment of temperature, trace species, and ozone in chemistry-climate model simulations of the recent past. *J. Geophys. Res.*, **111**, D22308, doi:10.1029/2006JD007327.
- Fu, Q., and K. N. Liou, 1992: On the correlated *k*-distribution method for radiative transfer in nonhomogeneous atmospheres. *J. Atmos. Sci.*, **49**, 2139–2156.
- Garrett, T. J., and Coauthors, 2005: Evolution of a Florida cirrus anvil. *J. Atmos. Sci.*, **62**, 2352–2372.

- , M. A. Zulauf, and S. K. Krueger, 2006: Effects of cirrus near the tropopause on anvil cirrus dynamics. *Geophys. Res. Lett.*, **33**, L17804, doi:10.1029/2006GL027071.
- Hartmann, D. L., and K. Larson, 2002: An important constraint on tropical cloud–climate feedback. *Geophys. Res. Lett.*, **29**, 1951, doi:10.1029/2002GL015835.
- , J. R. Holton, and Q. Fu, 2001: The heat balance of the tropical tropopause, cirrus, and stratospheric dehydration. *Geophys. Res. Lett.*, **28**, 1969–1972.
- Held, I. M., R. S. Hemler, and V. Ramaswamy, 1993: Radiative convective equilibrium with explicit two-dimensional moist convection. *J. Atmos. Sci.*, **50**, 3909–3927.
- Hong, G., P. Yang, B.-C. Gao, B. A. Baum, Y. X. Hu, M. D. King, and S. Platnick, 2007: High cloud properties from three years of MODIS *Terra* and *Aqua* collection-4 data over the tropics. *J. Appl. Meteor. Climatol.*, **46**, 1840–1856.
- Houze, R. A., and A. K. Betts, 1981: Convection in GATE. *Rev. Geophys.*, **19**, 541–576.
- Hurst, D. F., S. J. Oltmans, H. Voemel, K. H. Rosenlof, S. M. Davis, E. A. Ray, E. G. Hall, and A. F. Jordan, 2011: Stratospheric water vapor trends over Boulder, Colorado: Analysis of the 30 year boulder. *J. Geophys. Res.*, **116**, D02306, doi:10.1029/2010JD015065.
- Khairoutdinov, M. F., and D. A. Randall, 2003: Cloud resolving modeling of the arm summer 1997 IOP: Model formulation, results, uncertainties, and sensitivities. *J. Atmos. Sci.*, **60**, 607–625.
- Kley, D., P. J. Crutzen, H. G. J. Smit, H. Vomel, S. J. Oltmans, H. Grassl, and V. Ramanathan, 1996: Observations of near-zero ozone concentrations over the convective Pacific: Effects on air chemistry. *Science*, **274**, 230–233, doi:10.1126/science.274.5285.230.
- Krueger, S., and M. Zulauf, 2005: Radiatively-induced anvil spreading. *Proc. 15th Atmospheric Radiation Measurement (ARM) Science Team Meeting*, Daytona Beach, FL, DOE, 1–9. [Available online at [http://www.arm.gov/publications/proceedings/conf15/extended\\_abs/krueger\\_sk.pdf](http://www.arm.gov/publications/proceedings/conf15/extended_abs/krueger_sk.pdf).]
- Kuang, Z., and C. S. Bretherton, 2004: Convective influence on the heat balance of the tropical tropopause layer: A cloud-resolving model study. *J. Atmos. Sci.*, **61**, 2919–2927.
- , and D. L. Hartmann, 2007: Testing the fixed anvil temperature hypothesis in a cloud-resolving model. *J. Climate*, **20**, 2051–2057.
- Kubar, T. L., D. L. Hartmann, and R. Wood, 2007: Radiative and convective driving of tropical high clouds. *J. Climate*, **20**, 5510–5526.
- Lawrence, M., P. Crutzen, and P. Rasch, 1999: Analysis of the CEPEX ozone data using a 3D chemistry-meteorology model. *Quart. J. Roy. Meteor. Soc.*, **125**, 2987–3009.
- McFarlane, S. A., J. H. Mather, and T. P. Ackerman, 2007: Analysis of tropical radiative heating profiles: A comparison of models and observations. *J. Geophys. Res.*, **112**, D14218, doi:10.1029/2006JD008290.
- Mlawer, E. J., S. J. Taubman, P. D. Brown, M. J. Iacono, and S. A. Clough, 1997: Radiative transfer for inhomogeneous atmospheres: RRTM, a validated correlated-k model for the longwave. *J. Geophys. Res.*, **102** (D14), 16 663–16 682.
- Oman, L., D. W. Waugh, S. Pawson, R. S. Stolarski, and J. E. Nielsen, 2008: Understanding the changes of stratospheric water vapor in coupled chemistry-climate model simulations. *J. Atmos. Sci.*, **65**, 3278–3291.
- Pawson, S., and Coauthors, 2000: The GCM-Reality Intercomparison Project for SPARC (GRIPS): Scientific issues and initial results. *Bull. Amer. Meteor. Soc.*, **81**, 781–796.
- Rind, D., and P. Lonergan, 1995: Modeled impacts of stratospheric ozone and water-vapor perturbations with implications for high-speed civil transport aircraft. *J. Geophys. Res.*, **100** (D4), 7381–7396.
- Solomon, S., K. H. Rosenlof, R. W. Portmann, J. S. Daniel, S. M. Davis, T. J. Sanford, and G.-K. Plattner, 2010: Contributions of stratospheric water vapor to decadal changes in the rate of global warming. *Science*, **327**, 1219–1223, doi:10.1126/science.1182488.
- Thompson, A. M., and Coauthors, 2003: Southern Hemisphere Additional Ozonesondes (SHADOZ) 1998–2000 tropical ozone climatology 1. Comparison with Total Ozone Mapping Spectrometer (TOMS) and ground-based measurements. *J. Geophys. Res.*, **108** 8238, doi:10.1029/2001JD000967.
- , A. L. Allen, S. Lee, S. K. Miller, and J. C. Witte, 2011: Gravity and Rossby wave signatures in the tropical troposphere and lower stratosphere based on Southern Hemisphere Additional Ozonesondes (SHADOZ), 1998–2007. *J. Geophys. Res.*, **116**, D05302, doi:10.1029/2009JD013429.
- Tompkins, A. M., and G. C. Craig, 1999: Sensitivity of tropical convection to sea surface temperature in the absence of large-scale flow. *J. Climate*, **12**, 462–476.
- Xu, K., T. Wong, B. A. Wielicki, L. Parker, B. Lin, Z. A. Eitzen, and M. Branson, 2007: Statistical analyses of satellite cloud object data from CERES. Part II: Tropical convective cloud objects during 1998 El Niño and evidence for supporting the fixed anvil temperature hypothesis. *J. Climate*, **20**, 819–842.
- Zelinka, M. D., and D. L. Hartmann, 2010: Why is longwave cloud feedback positive? *J. Geophys. Res.*, **115**, D16117, doi:10.1029/2010JD013817.
- , and —, 2011: The observed sensitivity of high clouds to mean surface temperature anomalies in the tropics. *J. Geophys. Res.*, **116**, D23103, doi:10.1029/2011JD016459.